




Article

Increasing the Wear and Corrosion Resistance of a CP-Ti Surface by Plasma Electrolytic Borocarburing and Polishing

Marina A. Volosova, Sergei A. Kusmanov ^{*}, Ivan V. Tambovskiy, Tatiana L. Mukhacheva, Artem P. Mitrofanov , Igor V. Suminov and Sergey N. Grigoriev 

Department of High-Efficiency Processing Technologies, Moscow State University of Technology “STANKIN”, 127994 Moscow, Russia; m.volosova@stankin.ru (M.A.V.); i.tambovskiy@stankin.ru (I.V.T.); t_mukhacheva@ksu.edu.ru (T.L.M.); a.mitrofanov@stankin.ru (A.P.M.); i.suminov@stankin.ru (I.V.S.); s.grigoriev@stankin.ru (S.N.G.)

* Correspondence: sakusmanov@yandex.ru or s.kusmanov@stankin.ru; Tel.: +7-920-647-3090

Abstract: The paper examines the possibility of increasing the wear and corrosion resistance of a CP-Ti surface by duplex plasma electrolytic treatment (borocarburing and polishing). The structure and composition of diffusion layers, their microhardness, surface morphology and roughness, wear resistance during dry friction and corrosion resistance in Ringer’s solution were studied. The formation of a surface-hardened layer up to 200 μm thick with a microhardness of up to 950 HV, including carbides and a solid solution of boron and carbon, is shown. Subsequent polishing makes it possible to reduce surface roughness and remove weak areas of the porous oxide layer, which are formed during high-temperature oxidation in aqueous electrolyte vapor during borocarburing. Changing the morphology and structural-phase composition of the CP-Ti surface helps reduce weight wear by a factor of three (the mode of frictional interaction changes from microcutting to oxidative wear) and corrosion current density by a factor of four after borocarburing in a solution of boric acid, glycerin and ammonium chloride at 950 °C for 5 min and subsequent polishing in an ammonium fluoride solution at a voltage of 250 V for 3 min.

Keywords: CP-Ti; plasma electrolytic treatment; borocarburing; plasma electrolytic polishing; microhardness; surface roughness; wear resistance; corrosion resistance



Citation: Volosova, M.A.; Kusmanov, S.A.; Tambovskiy, I.V.; Mukhacheva, T.L.; Mitrofanov, A.P.; Suminov, I.V.; Grigoriev, S.N. Increasing the Wear and Corrosion Resistance of a CP-Ti Surface by Plasma Electrolytic Borocarburing and Polishing. *Surfaces* **2024**, *7*, 824–837. <https://doi.org/10.3390/surfaces7040054>

Received: 13 August 2024

Revised: 15 September 2024

Accepted: 4 October 2024

Published: 7 October 2024



Copyright: © 2024 by the authors. Licensee MDPI, Basel, Switzerland. This article is an open access article distributed under the terms and conditions of the Creative Commons Attribution (CC BY) license (<https://creativecommons.org/licenses/by/4.0/>).

1. Introduction

Titanium alloys have found wide application in various industries, such as the aircraft industry, rocket- and shipbuilding, medical and space technologies, the food industry, and the energy sector. This is primarily due to its lightness, ductility, and high corrosion resistance. Despite a number of advantages of titanium-based alloys as structural materials, their use as functional materials is limited by high toughness and low machinability, as well as low wear resistance. In particular, a feature of titanium and its alloys is a high tendency to contact seizure during friction. This property creates difficulties both in the processing of titanium by cutting and makes its use dangerous in friction units of mechanisms and machines due to the jamming of friction unit parts. To solve these problems, protective coatings are often used in functional components and mechanisms made of titanium materials. Among the widely used technologies for creating protective coatings are the spraying and fusion of wear-resistant coatings [1–7], and thermal and plasma electrolytic oxidation [8–22].

The intensive development of plasma electrolytic technologies has not ignored this issue. In addition to the previously mentioned plasma electrolytic oxidation, used to create protective ceramic-like coatings, there are two more types of the method, listed as follows: plasma electrolytic polishing and plasma electrolytic chemical–thermal treatment. Plasma electrolytic polishing is used on an ongoing basis to solve the challenges of reducing the roughness and decorating of metal surfaces, as well as removing coatings

from them [23–29]. Chemical–thermal treatment in electrolysis plasma solves the main problems of the traditional methods of chemical–thermal treatment (surface hardening and concomitant improvement in the mechanical characteristics of the surface and product), and can additionally be used to increase wear resistance and corrosion resistance due to the formation of a multiphase structures.

The known methods of hardening treatment have their limitations and disadvantages. The traditional methods of chemical–thermal treatment are characterized by a long diffusion saturation time. For example, to obtain a borated layer 0.1–0.3 mm thick on steels, saturation is carried out at 900–1100 °C for 5–6 h. Several operations are also required to carry out diffusion saturation, hardening, tempering, etc. Gas-flame surface hardening requires the manufacture of a multi-flame burner tip for each shape of the workpiece, since the shape of the heating flame must correspond to the shape of the surface being hardened. The flame is formed by the profile of the multi-flame burner tip. In addition, in order to harden the part, it is necessary to manufacture a separate sprinkler, which will form a linear, semi-ring, ring or complex-shaped profile of cooling jets. When performing surface hardening with contact heating by electric current, the hardened strips of the metal being processed can overlap each other, and in the overlap zone the metal will be subjected to repeated hardening, and in some parts to tempering, as a result of which the surface will be non-uniform in hardness. High-frequency current hardening requires the manufacture of an inductor in a shape consistent with the part being processed. A high-frequency current hardening unit costs 10–15 times more than a flame surface hardening unit.

The advantages of plasma electrolytic chemical-thermal treatment include the following:

- The possibility of obtaining promising nanoscale structures;
- High heating rates to the required diffusion saturation temperature (up to 100 °C/s), which prevent grain growth;
- The intensification of mass transfer and diffusion saturation due to the nature of the formed vapor–gas envelope around the workpiece, which leads to a reduction in processing time;
- The possibility of combining with hardening in one technological operation;
- The exclusion of finishing mechanical processing.

In addition, significant advantages of the plasma electrolytic chemical–thermal treatment and polishing are the small dimensions of the equipment, ease of operation and maintenance, the significantly lower cost compared to the traditional equipment of heat treatment workshops, and the possibility of processing local areas of the surfaces of parts. Plasma electrolytic polishing is successfully used for the finishing treatment of metals and alloys due to the high quality of the polished surface and the use of environmentally friendly and inexpensive aqueous solutions.

The largest amount of work in the field of plasma electrolytic chemical–thermal treatment has been carried out for the treatment of steels [30–42]. The effect of the complex effect of changes in the structural-phase composition and surface morphology on increasing wear resistance and corrosion resistance is shown. The processing of titanium alloys by plasma electrolytic chemical–thermal treatment has also been studied, but special cases of the processing of certain alloys were mainly considered [43–47]. Positive results were shown in increasing hardness, wear resistance and corrosion resistance. Among the types of processing considered, attention is paid to nitriding, carburizing and nitrocarburizing. Boriding is occasionally considered. In this work, it is proposed to expand the methods of diffusion saturation of titanium alloys—to study the process of joint saturation of CP-Ti with boron and carbon.

This work is aimed at studying the possibility of increasing the wear resistance of CP-Ti and changing its mechanism of friction and wear in the mating to eliminate the possibility of seizure and jamming. This treatment can effectively prevent friction seizure by changing the adhesive interaction of friction surfaces to a mechanical interaction. One of the key disadvantages of using plasma electrolytic treatment is the uncontrolled formation of a multiphase structure of the surface oxide layer, which can have significant irregularities,

as well as weak areas that are prone to peeling during operation, especially in frictional contact. In this regard, this work proposes a variant of complex surface treatment, which consists of plasma electrolytic chemical–thermal treatment and subsequent polishing. This technology will allow the finishing treatment to be carried out immediately after the hardening treatment, removing all the irregularities and weak areas of the outer oxide layer.

2. Materials and Methods

2.1. Materials

Cylindrical samples with a diameter of 10 mm and a height of 15 mm were used for the study. The samples were made of CP-Ti (0.25% Fe; 0.2% O, 0.1% Si; 0.07% C; 0.04% N; 0.01% H; and balance Ti). For the objectivity of the processing results, all samples were ground to a roughness of $Ra \sim 1.0 \mu\text{m}$.

2.2. Processing

Sequential plasma electrolytic borocarburing (PEBC) and plasma electrolytic polishing (PEP) processed the samples in the same electrolyzer (Figure 1).

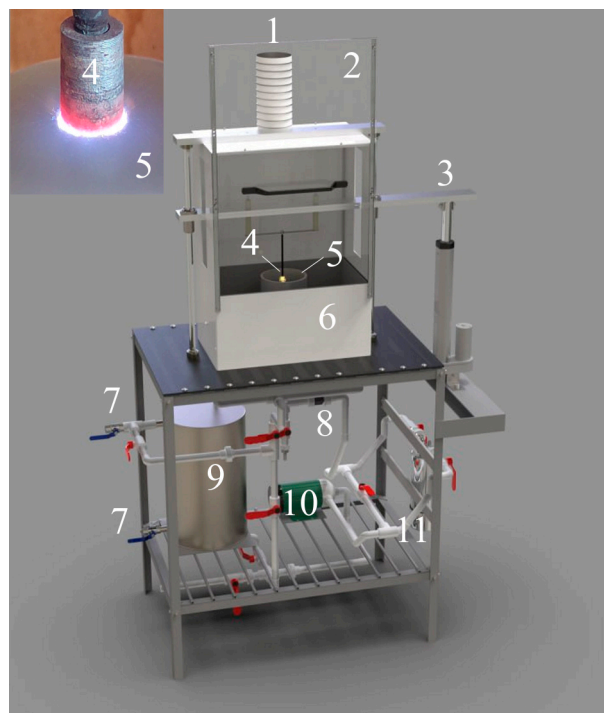


Figure 1. PEBC and PEP installation scheme: 1—ventilation duct; 2—protective screen of the working chamber; 3—linear drive; 4—workpiece–electrode (anode); 5—cylindrical cell–electrode (cathode); 6—working chamber; 7—valve with electric drive; 8—flow meter; 9—heat exchanger; 10—pump; 11—water filter.

The treatment was carried out with positive polarity of the samples in both PEBC and PEP. The electrolyte used for boron carburing was an aqueous solution of boric acid (3 wt.%), glycerol (8 wt.%) and ammonium chloride (10 wt.%). The electrolyte temperature was maintained constant at $22 \pm 2 \text{ }^\circ\text{C}$ by circulating through a heat exchanger. The PEBC temperature was 800, 850, 900, and 950 $^\circ\text{C}$. The treatment duration was 5 min. After diffusion saturation under these conditions, the samples were quenched in the electrolyte.

After borocarburing, the samples were polished in an electrolyte based on ammonium fluoride (4 wt.%). The electrolyte temperature was maintained at 90 $^\circ\text{C}$. The PEP duration was 1, 3, and 5 min at a voltage of 250 V.

2.3. Study of the Surface Phase Composition, Structure, Morphology and Properties

The phase composition of PEBC layers was determined using a PANalytical Empyrean X-ray diffractometer (XRD) (Malvern Panalytical, Malvern, UK) with $\text{CoK}\alpha$ radiation using PANalytical High Score Plus software (v. 2.0.0) [48] and ICCD PDF-2 and COD [49]. A Tescan Vega 3 scanning electron microscope (SEM) (Tescan, Brno, Czech Republic) was used to study the structural features of the surface layers of CP-Ti samples after PEBC. Microhardness measurements of the PEBC layers were performed using a Falcon 503 microhardness tester (Innovatest Europe BV, Maastricht, The Netherlands) under a load of 0.1 N. A Micromed MET metallographic microscope (Observing devices, St. Petersburg, Russia) was used to analyze the surface morphology and friction tracks. A Hommel tester t8000 profilometer (Jenoptik, Jena, Germany) was used to measure the surface roughness after PEBC and PEP.

Tribological tests were carried out according to the scheme shown in Figure 2. The side surface of the samples was subjected to friction, which was in contact with a counter body made of tool alloy steel (wt.%: 0.9–1.2 Cr, 1.2–1.6 W, 0.8–1.1 Mn, and 0.9–1.05 C) in the form of a plate with a semicircular recess. The sample rotated in the dry friction mode with a sliding speed of 1.555 m/s under a load of 10 N over a distance of 1000 m. The temperature in the frictional contact zone was measured using a digital infrared thermometer MLX90614 (Melexis Electronic Technology, Shanghai, China).

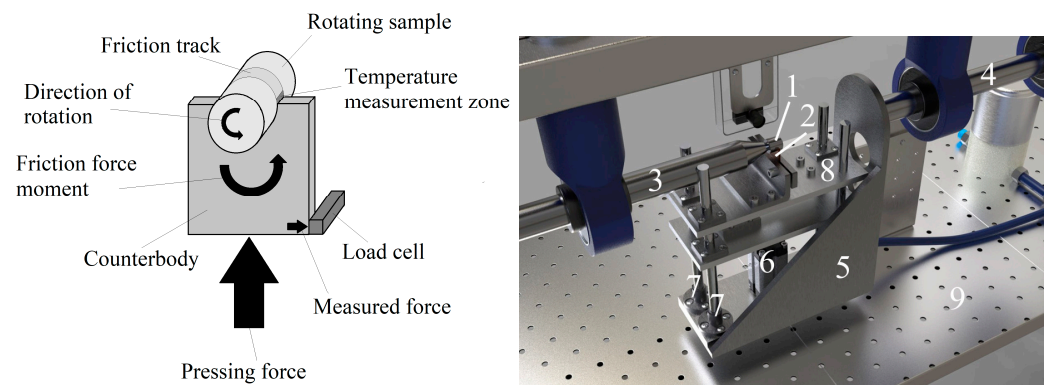


Figure 2. Friction scheme and unit: 1—cylindrical sample; 2—counter body; 3, 4—shaft; 5—crank; 6—pneumatic cylinder; 7—guides; 8—table; 9—strain gauges.

Corrosion tests were performed using a Biologic SP-150 potentiostat–galvanostat (Biologic Science Instruments, France). A standard three-electrode cell in Ringer’s solution (8.6 g/L NaCl, 0.3 g/L KCl, 0.25 g/L CaCl_2) was used. Graphite was the auxiliary electrode, and a silver chloride electrode was used as a reference electrode.

3. Results and Discussion

3.1. Structure, Composition, Morphology and Roughness of CP-Ti Surface after PEBC

During the PEBC, the processes of high-temperature oxidation, anodic dissolution and diffusion saturation simultaneously occur on the surface, which is typical for anodic plasma electrolytic chemical–thermal treatment [40,41]. The result of high-temperature oxidation was the formation of an oxide layer containing many pores, the sizes of which increase with increasing treatment temperature (Figure 3). The composition of the oxide layer, according to X-ray analysis, includes the oxides of the composition $\text{TiO}_{0.325}$, TiO_2 (rutile and anatase) and Ti_3O (Figure 4). With an increase in the PEBC temperature, there is an increase in the proportion of higher oxides TiO_2 (rutile and anatase) and a decrease in the proportion of lower oxides $\text{TiO}_{0.325}$ and Ti_3O (Table 1).

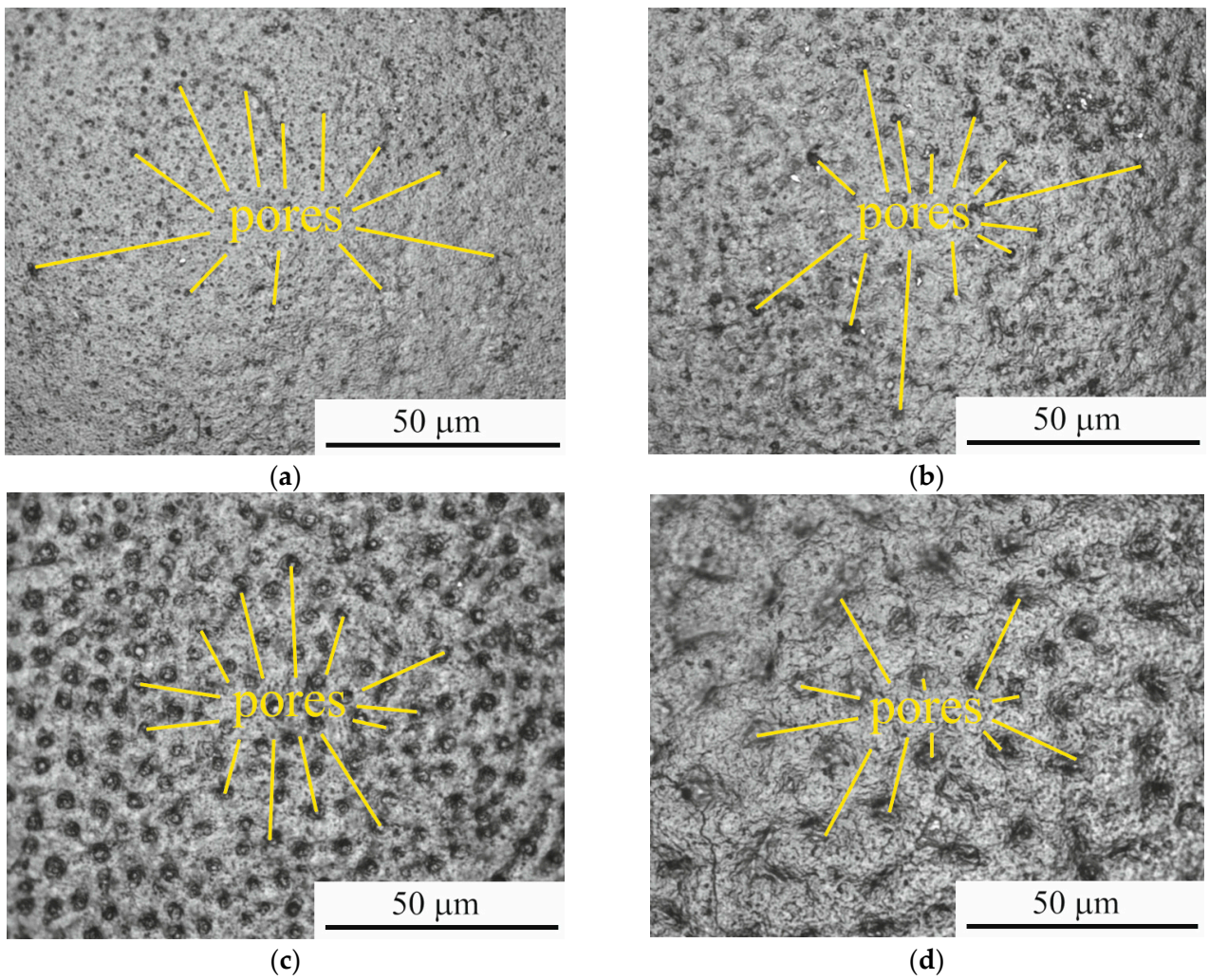


Figure 3. Surface morphology of CP-Ti samples after PEBC at different temperatures: (a) 800 °C; (b) 850 °C; (c) 900 °C; (d) 950 °C.

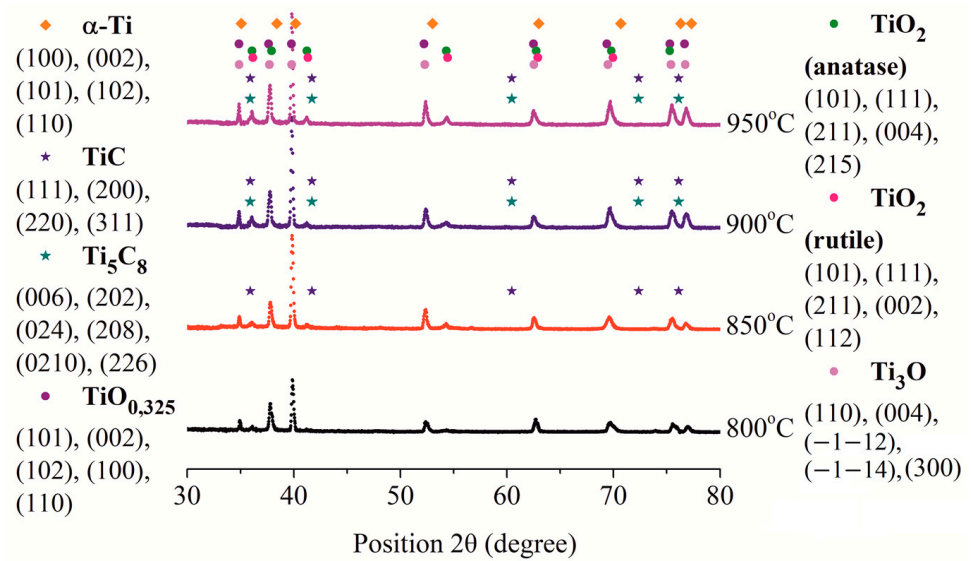


Figure 4. X-ray diffraction pattern of the surface of CP-Ti samples after PEBC at different temperatures.

Table 1. Characteristics of phase fractions for sample after PEBC at different temperatures.

Chemical Formula	Crystal System	Volume of Cell ($10^6 \mu\text{m}^3$)	Phase Fraction (%)			
			800 °C	850 °C	900 °C	950 °C
α -Ti	Hexagonal	35.32	35	31	27	20
Ti ₃ O	Hexagonal	218.22	27	24	20	21
TiO ₂ (anatase)	Tetragonal	135.25	7	9	6	10
TiO ₂ (rutile)	Tetragonal	62.07	5	6	8	9
TiO _{0.325}	Hexagonal	36.48	26	20	24	18
TiC	Cubic	81.07	–	10	8	12
Ti ₈ C ₅	Rhombohedral	486.48	–	–	7	10

Anodic processes involve the electrochemical dissolution of the surface, leading to weight loss in the samples (Table 2) and influencing their morphology. In this case, we can talk about competition between the processes of oxidation and anodic dissolution. When surface oxidation dominates, an increase in roughness is observed, and when anodic dissolution prevails, the opposite trend is observed. The surface roughness R_a of samples after PEBC at 950 °C increases from $1.00 \pm 0.10 \mu\text{m}$ (untreated sample) to $1.27 \pm 0.56 \mu\text{m}$ (Table 2). At lower processing temperatures, surface roughness decreases. The maximum reduction in average roughness to $0.46 \pm 0.09 \mu\text{m}$ is observed after PEBC at 800 °C, which is two times lower than that of the untreated sample. Further, with increasing processing temperature, the roughness increases because of the intensification of high-temperature oxidation. The data obtained indicate the predominance of anodic dissolution at temperatures of 800, 850 and 900 °C and high-temperature oxidation at 950 °C.

Table 2. The values of weight loss of samples during PEBC, surface roughness, temperature in the tribological contact zone, friction coefficient, weight wear and corrosion current density after PEBC at different temperatures.

PEBC Temperature (°C)	Weight Loss (mg)	Surface Roughness R_a (μm)	Temperature in the Tribological Contact Zone (°C)	Friction Coefficient	Weight Wear (mg)	Corrosion Current Density ($\mu\text{A}/\text{cm}^2$)
Untreated		1.00 ± 0.10	56.0	0.465 ± 0.005	3.70 ± 0.04	0.32
800	2.7	0.46 ± 0.10	68.2	0.341 ± 0.003	1.65 ± 0.02	0.38
850	3.4	0.56 ± 0.18	69.0	0.399 ± 0.004	2.48 ± 0.03	1.27
900	4.2	0.61 ± 0.26	75.4	0.418 ± 0.004	3.03 ± 0.04	1.62
950	17.0	1.27 ± 0.56	73.3	0.393 ± 0.004	3.95 ± 0.05	1.78

SEM analysis reveals that diffusion saturation leads to the formation of a PEBC layer beneath the surface oxide layer (Figure 5). X-ray analysis shows that this layer contains titanium carbide and a solid solution of diffusants (Figure 4). Metallographically, PEBC layer consists of an unetched carbide layer and a diffusion layer. The resulting PEBC layer has increased microhardness, which increases with increasing PEBC temperature and is more than three times higher than the value of the initial microhardness (Figure 6). The increase in hardness correlates with the increase in the proportion of carbides in the surface layer (Table 1). The thickness of the hardened layer, in turn, after treatment at 950 °C reaches 200 μm .

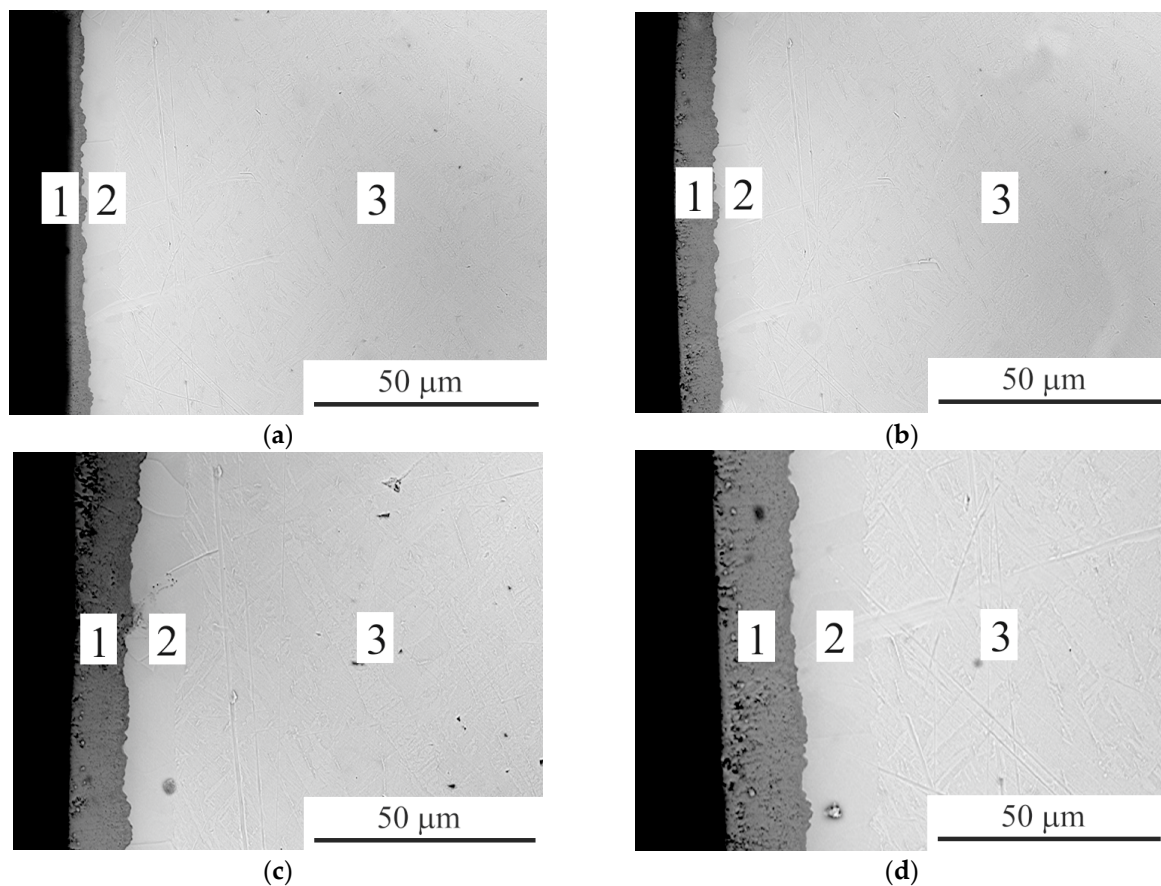


Figure 5. SEM image of the cross section of CP-Ti samples after PEBC at different temperatures: (a) 800 °C; (b) 850 °C; (c) 900 °C; (d) 950 °C. 1—oxide layer; 2—PEBC layer; 3—initial structure.

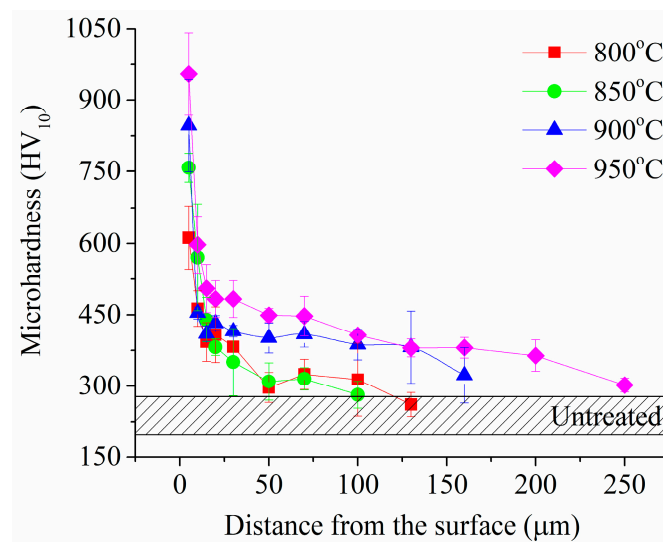


Figure 6. Microhardness of the surface layer of CP-Ti samples after PEBC at different temperatures.

3.2. Tribological Properties of CP-Ti Surface after PEBC

As a result of tribological tests after treatment at all temperatures of PEBC, the friction coefficient decreases compared to the untreated sample (Table 2). The greatest reduction in the friction coefficient occurs after PEBC at 800 °C. It is under these conditions that the minimum wear rate is observed.

An increase in the treatment temperature entails a linear increase in weight wear, which, on samples after treatment at 950 °C, exceeds the value of the untreated sample. In

this case, the friction coefficient also increases and has similar values in the temperature range from 850 to 950 °C.

An increase in weight wear with increasing processing temperature can be associated with an increase in the porosity of the oxide layer, which will be destroyed by friction. The analysis of the morphology of the friction tracks reveals that the samples experience oxidative wear after PEBC (Figure 7). In contrast, the untreated sample's friction tracks show not only signs of oxidative wear but also evidence of microcutting. In this case, the oxide layer formed during PEBC will wear off and prevent the rapid destruction of oxidation products during tribocoupling, which have a lubricating effect when sliding surfaces. When testing an untreated sample, this does not happen; oxidation products during friction are quickly destroyed and the material is destroyed by cutting by wear products.

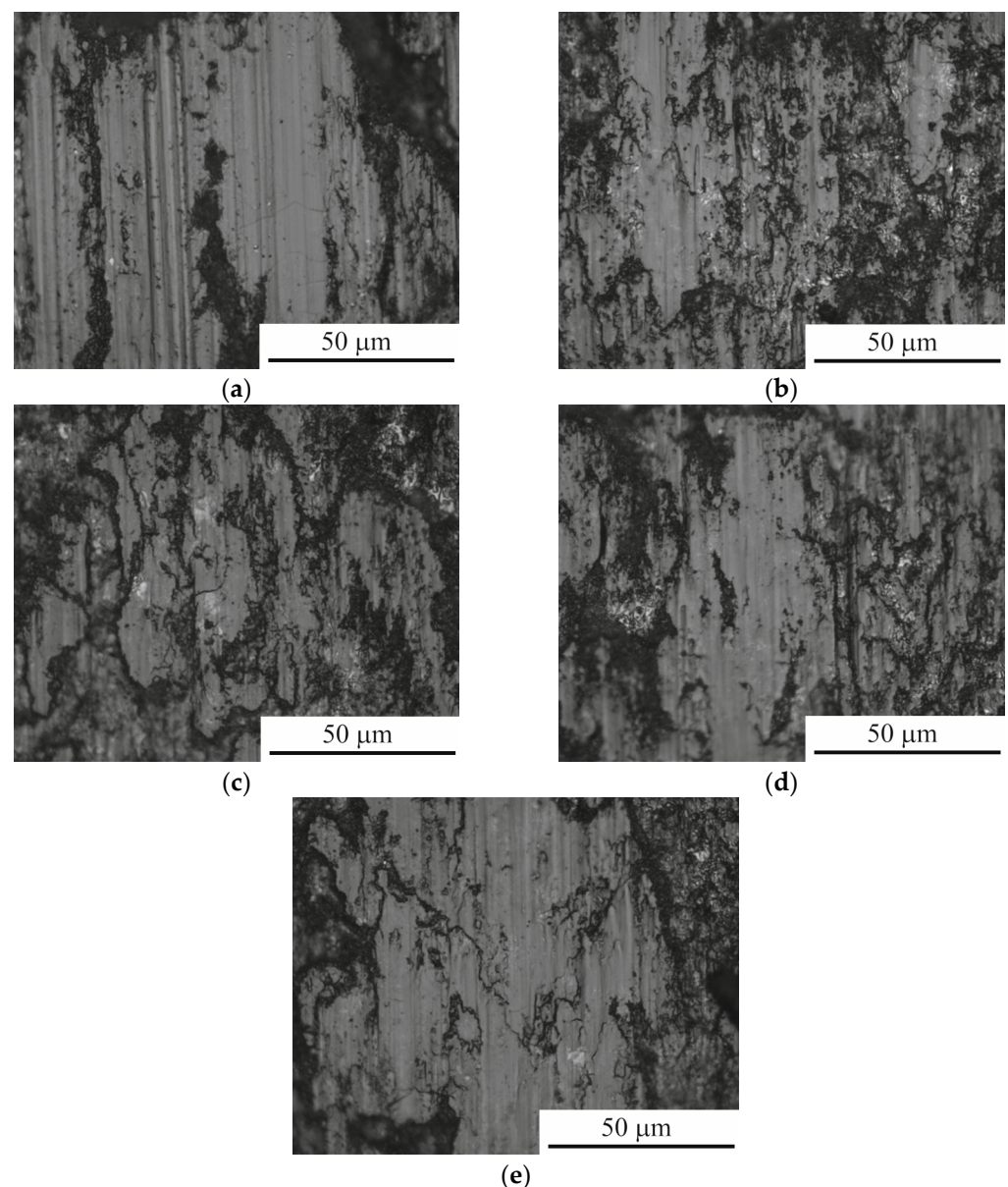


Figure 7. Morphology of friction tracks of CP-Ti samples before (a) and after PEBC at different temperatures: (b) 800 °C; (c) 850 °C; (d) 900 °C; (e) 950 °C.

3.3. Corrosion Properties of CP-Ti Surface after PEBC

The results of corrosion tests in Ringer's solution showed an increase in corrosion current density after PEBC (Table 2). A close value of the corrosion current to the initial

surface is observed only on samples processed at a temperature of 800 °C. An increase in the PEBC temperature leads to an increase in the corrosion current. This pattern can be associated with the development of surface relief—an increase in the porosity of the oxide layer, which will accumulate corrosive agents. In this case, a correlation between the corrosion current density and surface roughness is observed.

Thus, to obtain a surface with maximum microhardness, it is more expedient to carry out PEBC at a temperature of 950 °C. The tribological and corrosion properties of PEBC samples will be determined primarily by the surface morphology, which in fact represents the morphology of the oxide layer. The outer oxide layer, which influences the tribological and corrosion behavior of the surface, can be partially or completely removed using PEP. We propose to study the effect of PEP on surface properties by using samples treated at a temperature of 950 °C, which exhibit maximum microhardness.

3.4. Structure, Composition, Morphology and Roughness of CP-Ti Surface after Duplex Processing (PEBC+PEP)

Polishing in an ammonium fluoride solution for varying durations showed that after 1 min of PEP, the process removes the visible pores of the oxide layer (Figure 8b), while simultaneously increasing the surface roughness (Table 3). Increasing the PEP duration to 3 min made it possible to significantly smooth out the surface relief (Figure 8c) and reduce roughness. After 5 min of polishing, the oxide layer is completely removed (Figure 8d), and the roughness increases slightly.

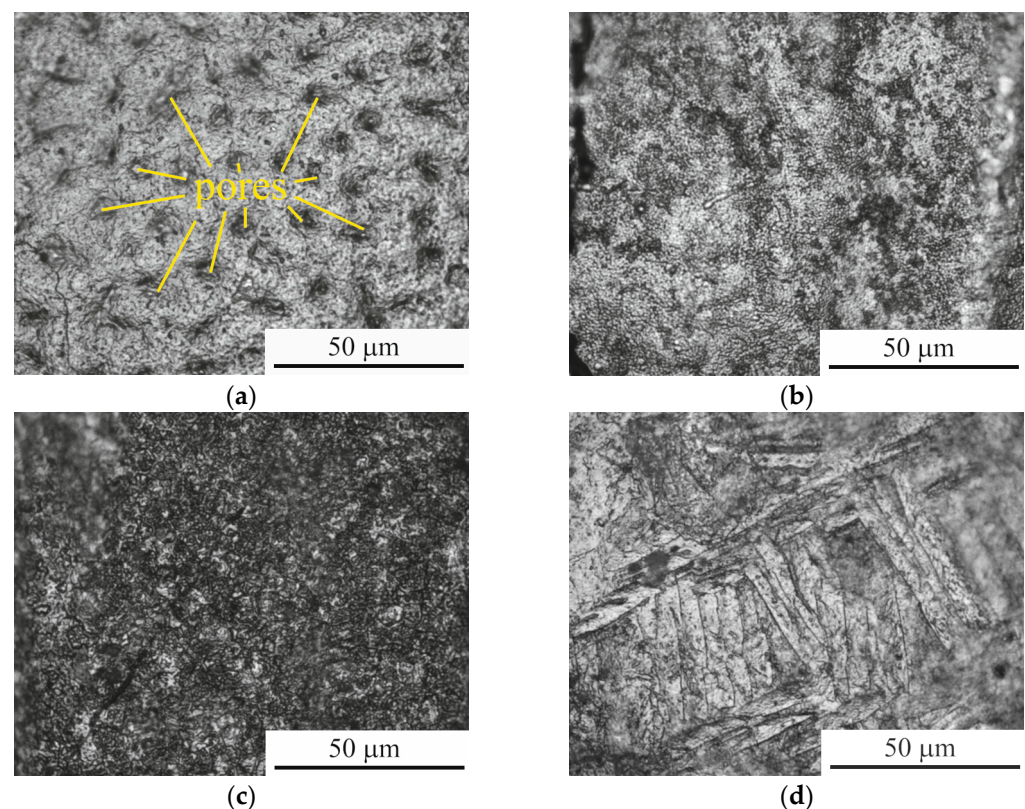


Figure 8. Surface morphology of CP-Ti samples before (a) and after PEP at different times: (b) 1 min; (c) 3 min; (d) 5 min.

Microhardness measurements indicated that the polishing process preserves the hardened layer after 1 and 3 min (Figure 9). The X-ray analysis data reveal a decrease in the intensity of titanium oxide peaks (Figure 10) and changes in their fractional composition (Table 4). Increasing the PEP duration to 5 min leads to the removal of part of the hardened layer and a decrease in microhardness (Figure 9). A decrease in the proportion of titanium carbides indicates the partial dissolution of the hardened layer (Table 4).

Table 3. The values of surface roughness, temperature in the tribological contact zone, friction coefficient, weight wear and corrosion current density after PEP at different times.

PEP Time (min)	Surface Roughness R_a (μm)	Temperature in the Tribological Contact Zone ($^{\circ}\text{C}$)	Friction Coefficient	Weight Wear (mg)	Corrosion Current Density ($\mu\text{A}/\text{cm}^2$)
Untreated	1.00 ± 0.10	56.0	0.465 ± 0.005	3.70 ± 0.04	0.32
Before PEP	1.27 ± 0.56	73.3	0.393 ± 0.004	3.95 ± 0.05	1.78
1	1.38 ± 0.41	81	0.248 ± 0.002	1.40 ± 0.02	0.34
3	0.61 ± 0.09	83	0.231 ± 0.002	1.22 ± 0.02	0.08
5	0.67 ± 0.08	59	0.331 ± 0.003	1.69 ± 0.03	0.16

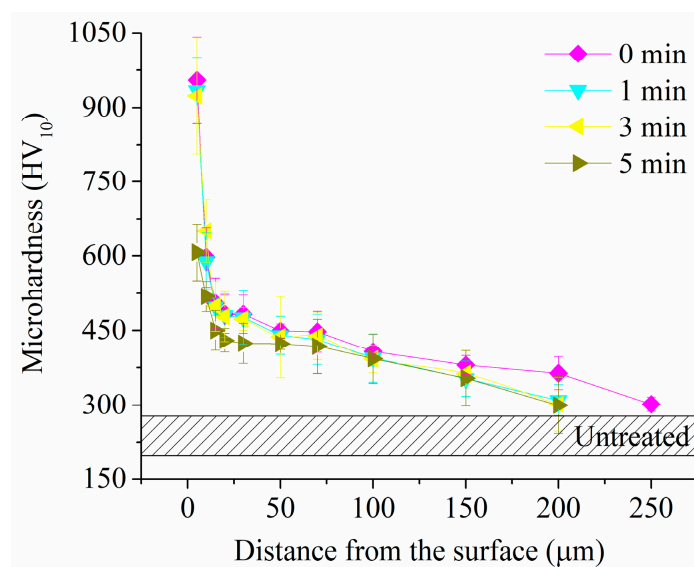


Figure 9. The microhardness of the surface layer of CP-Ti samples before (0 min) and after PEP at different times.

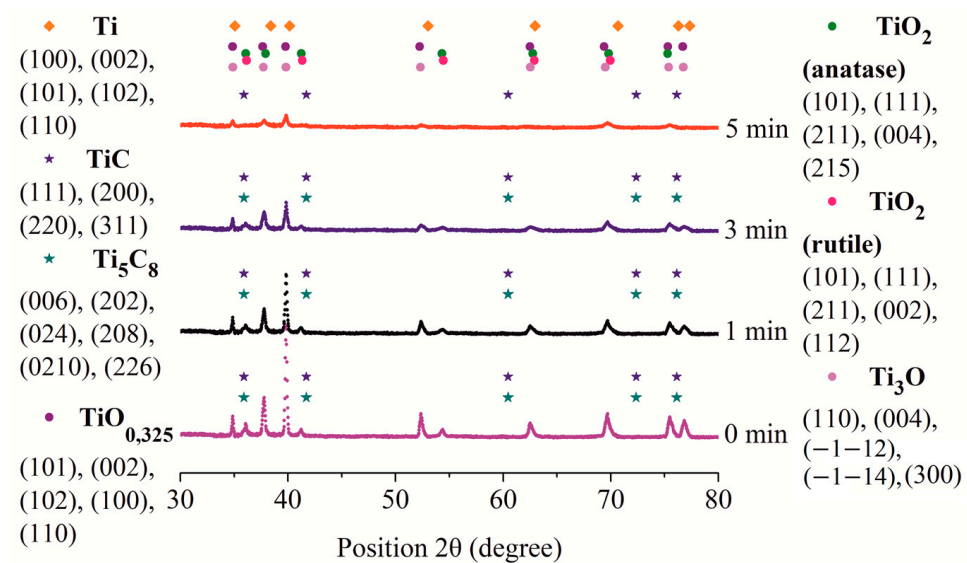


Figure 10. The X-ray diffraction pattern of the surface of CP-Ti samples before (0 min) and after PEP at different times.

Table 4. Characteristics of phase fractions for samples after PEP at different times.

Chemical Formula	Crystal System	Volume of Cell ($10^6 \mu\text{m}^3$)	Phase Fraction (%)			
			0 min	1 min	3 min	5 min
α -Ti	Hexagonal	35.32	20	37	41	56
Ti ₃ O	Hexagonal	218.22	21	16	14	15
TiO ₂ (anatase)	Tetragonal	135.25	10	8	9	7
TiO ₂ (rutile)	Tetragonal	62.07	9	6	7	8
TiO _{0.325}	Hexagonal	36.48	18	16	12	8
TiC	Cubic	81.07	12	9	10	6
Ti ₈ C ₅	Rhombohedral	486.48	10	8	7	–

3.5. Tribological Properties of CP-Ti Surface after Duplex Treatment (PEBC+PEP)

Tribological tests revealed that polishing PEBC samples resulted in a decrease in the friction coefficient (Table 3). Samples subjected to PEBC followed by PEP for 3 min demonstrate the largest reduction in the friction coefficient, decreasing from 0.393 to 0.231. In this case, weight wear is also minimal, 3.1 times lower compared to the untreated sample and 3.3 times lower compared to the PEBC sample.

After PEP for 1 and 3 min, dark oxide films are visible on the friction tracks (Figure 11). Oxide films shielding the friction contact surfaces have lower hardness than the surface hardened layer of the sample. This leads to the fact that during friction it is removed from the surface of a metal body more easily than the surface layer. Wear occurs because of the removal of the oxidized layer. In addition, the oxide film can act as a friction lubricant. After five minutes of polishing, the leading wear mechanism changes. The photograph of the friction track shows stripes in the sliding direction without sharp boundaries, showing the plastic deformation of the base metal by the roughness protrusions of the counter body. There are practically no traces of dark oxide films in the photographic field and wear occurs directly along the metal base material, which explains the higher values of both the friction coefficient and weight wear.

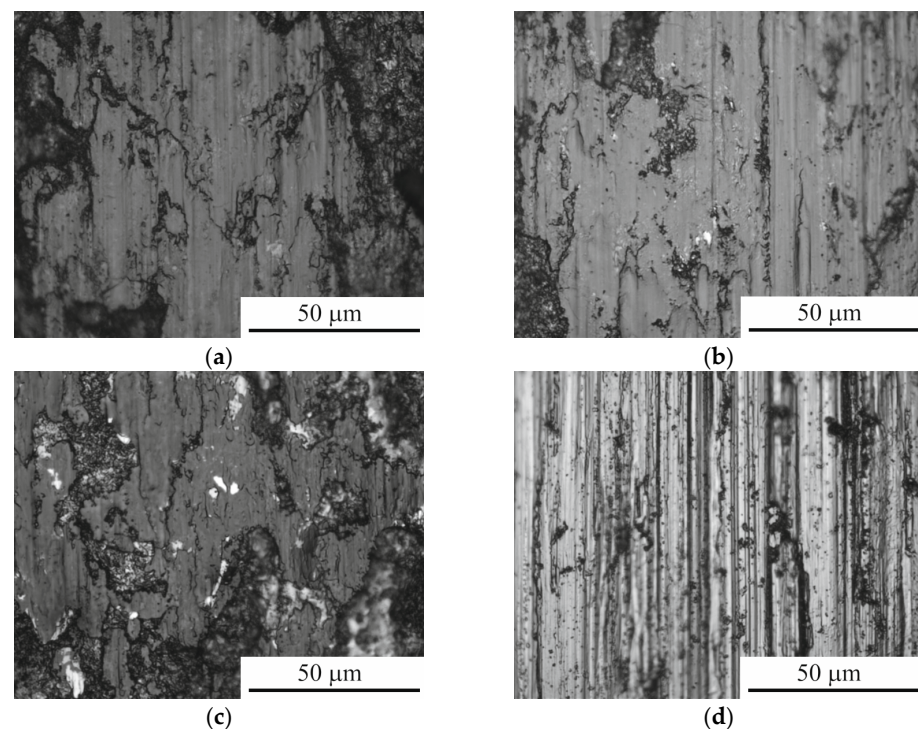


Figure 11. Morphology of friction tracks of CP-Ti samples before (a) and after PEP at different times: (b) 1 min; (c) 3 min; (d) 5 min.

3.6. Corrosion Properties of CP-Ti Surface after Duplex Treatment (PEBC+PEP)

Subsequent PEP of the PEBC surface in an ammonium fluoride solution favors a decrease in the corrosion current density (Table 3). After just 1 min of polishing, the corrosion current decreases by 5.2 times and becomes close to the value of the untreated sample. The greatest reduction occurs after 3 min of PEP—the corrosion current density becomes 22.2 times lower than the PEBC surface and 4 times lower than the untreated surface. After 5 min of PEP, there is an increase in corrosion current density, but to a lower value than that of the untreated sample.

The results obtained indicate a correlation between corrosion current density and morphology and roughness surface. The formation of a morphologically homogeneous surface, including oxides and with low roughness, will determine the corrosion resistance of the PEBC surface of CP-Ti.

4. Conclusions

Based on the results of the work, a variant of complex treatment of the surface of CP-Ti was proposed, consisting of PEBC and subsequent PEP. This technology makes it possible to form a hardened layer on the surface of CP-Ti, including carbides and a solid solution of boron and carbon. Polishing in electrolysis plasma in the same electrolyzer after hardening treatment makes it possible to remove the unevenness and the weak areas of the outer porous oxide layer. A comprehensive reduction in roughness and surface hardening contributes to increased wear resistance and corrosion resistance.

The plasma electrolytic treatment of CP-Ti effectively prevents seizure during friction, changing the adhesive interaction of friction surfaces to a mechanical interaction. Changing the mechanism of friction and wear of samples from CP-Ti in conjunction with hardened tool steel allows for the use of the technology of plasma electrolytic treatment to improve the friction units consisting of titanium and steel elements. The conditions of dry friction considered in the work and applied to the studied materials have a wide range of applications in mechanical engineering, aircraft manufacturing, and medicine, as well as in the food industry and other industries.

We have obtained results, based on which it is possible to optimize the modes of PEBC and PEP for the operation of products from CP-Ti in specific conditions. Additionally, researchers can extend the results obtained from CP-Ti, as a model variant, to other titanium alloys, presenting a promising avenue for further research.

Among the unsolved problems, it is necessary to expand the conditions of tribological and corrosion tests to determine the limitations of the proposed technology's efficiency. Additionally, the researchers have not fully disclosed the fundamental component; a more in-depth study of the mechanisms of physical and chemical processes and their influence on the formation of the modified surface holds scientific interest.

Author Contributions: Conceptualization, M.A.V. and S.A.K.; methodology, S.A.K.; validation, M.A.V.; formal analysis, I.V.S.; investigation, I.V.T., T.L.M. and A.P.M.; resources, S.N.G.; writing—original draft preparation, M.A.V., I.V.T., T.L.M. and I.V.S.; writing—review and editing, S.A.K. and S.N.G.; visualization, S.A.K. and A.P.M.; supervision, I.V.S.; project administration, S.N.G.; funding acquisition, M.A.V. All authors have read and agreed to the published version of the manuscript.

Funding: This research was carried out with the financial support of the Russian Science Foundation within the framework of scientific project No. 24-19-00811.

Data Availability Statement: The original contributions presented in the study are included in the article, further inquiries can be directed to the corresponding author.

Acknowledgments: This study was carried out on the equipment of the Center of Collective Use “State Engineering Center” of MSUT “STANKIN” supported by the Ministry of Higher Education of the Russian Federation (project 075-15-2021-695 from 26 July 2021, unique identifier RF 2296.61321X0013).

Conflicts of Interest: The authors declare no conflicts of interest.

References

1. Fan, M.; Du, P.; Wen, K.; Zhang, R.; Yu, S.; Chen, T. Tribological Properties of Laser-Cladded NiCrBSi Coatings Undergoing Friction with Ti6Al4V Alloys. *Coatings* **2024**, *14*, 813. [[CrossRef](#)]
2. Wang, G.; Liu, J.; Yang, J.; Liu, S.; Bu, L.; Chen, J. Study of the Performance of Laser Melting Wear-Resistant Coatings on TC4 Titanium Alloy Surfaces. *Coatings* **2024**, *14*, 730. [[CrossRef](#)]
3. Zhao, Q.; Wang, L.; Hu, T.; Song, J.; Su, Y.; Hu, L. Research on the Preparation of Zirconia Coating on Titanium Alloy Surface and Its Tribological Properties. *Lubricants* **2024**, *12*, 154. [[CrossRef](#)]
4. He, Q.; Saciotto, V.; DePaiva, J.M.; Guimaraes, M.C.; Kohlscheen, J.; Martins, M.M.; Veldhuis, S.C. Enhancing Tool Performance in High-Speed End Milling of Ti-6Al-4V Alloy: The Role of AlCrN PVD Coatings and Resistance to Chipping Wear. *J. Manuf. Mater. Process.* **2024**, *8*, 68. [[CrossRef](#)]
5. AbuAlia, M.; Fullam, S.; Cinotti, F.; Manninen, N.; Wimmer, M.A. Titanium Nitride Coatings on CoCrMo and Ti6Al4V Alloys: Effects on Wear and Ion Release. *Lubricants* **2024**, *12*, 96. [[CrossRef](#)]
6. Men, B.; Sun, S.; Hu, C.; Zhang, Q.; Han, B. Microstructure and Wear Resistance of Si-TC4 Composite Coatings by High-Speed Wire-Powder Laser Cladding. *Materials* **2024**, *17*, 1126. [[CrossRef](#)]
7. Liu, Z.; Ren, S.; Li, T.; Chen, P.; Hu, L.; Wu, W.; Li, S.; Liu, H.; Li, R.; Zhang, Y. A Comparison Study on the Microstructure, Mechanical Features, and Tribological Characteristics of TiN Coatings on Ti6Al4V Using Different Deposition Techniques. *Coatings* **2024**, *14*, 156. [[CrossRef](#)]
8. Xu, Y.; Jiang, Y.; Xie, J.; Xu, Q.; Fei, H.; Lu, Y.; Gong, J. Effect of Temperature, Vacuum Condition and Surface Roughness on Oxygen Boost Diffusion of Ti-6Al-4V Alloy. *Coatings* **2024**, *14*, 314. [[CrossRef](#)]
9. Wang, Q.; Song, P.; Niu, W.; Li, N.; Hu, N. High Temperature Oxidation Behavior of Additive Manufactured Ti6Al4V Alloy with the Addition of Yttrium Oxide Nanoparticles. *Materials* **2024**, *17*, 2544. [[CrossRef](#)]
10. Grigoriev, S.; Peretyagin, N.; Apelfeld, A.; Smirnov, A.; Morozov, A.; Torskaya, E.; Volosova, M.; Yanushevich, O.; Yarygin, N.; Krikheli, N.; et al. Investigation of Tribological Characteristics of PEO Coatings Formed on Ti6Al4V Titanium Alloy in Electrolytes with Graphene Oxide Additives. *Materials* **2023**, *16*, 3928. [[CrossRef](#)]
11. Marcuz, N.; Ribeiro, R.P.; Rangel, E.C.; Cristino da Cruz, N.; Correa, D.R.N. The Effect of PEO Treatment in a Ta-Rich Electrolyte on the Surface and Corrosion Properties of Low-Carbon Steel for Potential Use as a Biomedical Material. *Metals* **2023**, *13*, 520. [[CrossRef](#)]
12. Apelfeld, A.; Grigoriev, S.; Krit, B.; Ludin, V.; Suminov, I.; Chudinov, D. Improving the stability of the coating properties for group plasma electrolytic oxidation. *Manuf. Lett.* **2022**, *33*, 54. [[CrossRef](#)]
13. Aliofkhaezaei, M.; Macdonald, D.D.; Matykina, E.; Parfenov, E.V.; Egorin, V.S.; Curran, J.A.; Troughton, S.C.; Sinebryukhov, S.L.; Gnednikov, S.V.; Lampke, T.; et al. Review of plasma electrolytic oxidation of titanium substrates: Mechanism, properties, applications and limitations. *Appl. Surf. Sci. Adv.* **2021**, *5*, 100121. [[CrossRef](#)]
14. Grigoriev, S.; Peretyagin, N.; Apelfeld, A.; Smirnov, A.; Rybkina, A.; Kameneva, E.; Zheltukhin, A.; Gerasimov, M.; Volosova, M.; Yanushevich, O.; et al. Investigation of the Characteristics of MAO Coatings Formed on Ti6Al4V Titanium Alloy in Electrolytes with Graphene Oxide Additives. *J. Compos. Sci.* **2023**, *7*, 142. [[CrossRef](#)]
15. Jin, S.; Ma, X.; Wu, R.; Wang, G.; Zhang, J.; Krit, B.; Betsofen, S.; Liu, B. Advances in micro-arc oxidation coatings on Mg-Li alloys. *Appl. Surf. Sci. Adv.* **2022**, *8*, 100219. [[CrossRef](#)]
16. Bogdashkina, N.L.; Gerasimov, M.V.; Zalavutdinov, R.K.; Kasatkina, I.V.; Krit, B.L.; Lyudin, V.B.; Fedichkin, I.D.; Shcherbakov, A.I.; Apelfeld, A.V. Influence of Nickel Sulfate Additives to Electrolytes Subjected to Microarc Oxidation on the Structure, Composition, and Properties of Coatings Formed on Titanium. *Surf. Eng. Appl. Electrochem.* **2018**, *54*, 331–337. [[CrossRef](#)]
17. Bordbar-Khiabani, A.; Ebrahimi, S.; Yarmand, B. Highly corrosion protection properties of plasma electrolytic oxidized titanium using rGO nanosheets. *Appl. Surf. Sci.* **2019**, *486*, 153–165. [[CrossRef](#)]
18. Kim, S.-P.; Kaseem, M.; Choe, H.-C. Plasma electrolytic oxidation of Ti-25Nb-xTa alloys in solution containing Ca and P ions. *Surf. Coat. Technol.* **2020**, *395*, 125916. [[CrossRef](#)]
19. Maltanova, H.; Stojadinovic, S.; Vasilic, R.; Karpushenkov, S.; Belko, N.; Samtsov, M.; Poznyak, S. Photoluminescent Coatings on Zinc Alloy Prepared by Plasma Electrolytic Oxidation in Aluminate Electrolyte. *Coatings* **2023**, *13*, 848. [[CrossRef](#)]
20. Stojadinović, S.; Jovović, J.; Petković, M.; Vasilic, R.; Konjević, N. Spectroscopic and Real-Time Imaging Investigation of Tantalum Plasma Electrolytic Oxidation (PEO). *Surf. Coat. Technol.* **2011**, *205*, 5406–5413. [[CrossRef](#)]
21. Hariprasad, S.; Ashfaq, M.; Arunnellaiappan, T.; Harilal, M.; Rameshbabu, N. Role of electrolyte additives on in-vitro corrosion behavior of DC plasma electrolytic oxidation coatings formed on Cp-Ti. *Surf. Coat. Technol.* **2016**, *292*, 20–29. [[CrossRef](#)]
22. Venkateswarlu, K.; Rameshbabu, N.; Sreekanth, D.; Bose, A.C.; Muthupandi, V.; Subramanian, S. Fabrication and characterization of micro-arc oxidized fluoride containing titania films on Cp-Ti. *Ceram. Int.* **2013**, *39*, 801–812. [[CrossRef](#)]
23. Schorn, L.; Wilkat, M.; Lommen, J.; Borelli, M.; Muhammad, S.; Rana, M. Plasma Electrolytic Polished Patient-Specific Orbital Implants in Clinical Use—A Technical Note. *J. Pers. Med.* **2023**, *13*, 148. [[CrossRef](#)]
24. Danilov, I.; Hackert-Oschatzchen, M.; Zinecker, M.; Meichsner, G.; Edelmann, J.; Schubert, A. Process Understanding of Plasma Electrolytic Polishing through Multiphysics Simulation and Inline Metrology. *Micromachines* **2019**, *10*, 214. [[CrossRef](#)] [[PubMed](#)]
25. Navickaitė, K.; Ianniciello, L.; Tušek, J.; Engelbrecht, K.; Bahl, C.R.H.; Penzel, M.; Nestler, K.; Böttger-Hiller, F.; Zeidler, H. Plasma Electrolytic Polishing of Nitinol: Investigation of Functional Properties. *Materials* **2021**, *14*, 6450. [[CrossRef](#)]

26. Nestler, K.; Böttger-Hiller, F.; Adamitzki, W.; Glowa, G.; Zeidler, H.; Schubert, A. Plasma electrolytic polishing—An overview of applied technologies and current challenges to extend the polishable material range. *Procedia CIRP* **2016**, *42*, 503–507. [[CrossRef](#)]
27. Ma, G.; Li, S.; Liu, X.; Yin, X.; Jia, Z.; Liu, F. Combination of Plasma Electrolytic Processing and Mechanical Polishing for Single-Crystal 4H-SiC. *Micromachines* **2021**, *12*, 606. [[CrossRef](#)]
28. Parfenov, E.V.; Farrakhov, R.G.; Mukaeva, V.R.; Gusarov, A.V.; Nevyantseva, R.R.; Yerokhin, A. Electric field effect on surface layer removal during electrolytic plasma polishing. *Surf. Coat. Technol.* **2016**, *307*, 1329–1340. [[CrossRef](#)]
29. Stepputat, V.N.; Zeidler, H.; Safranchik, D.; Strokin, E.; Böttger-Hiller, F. Investigation of Post-Processing of Additively Manufactured Nitinol Smart Springs with Plasma-Electrolytic Polishing. *Materials* **2021**, *14*, 4093. [[CrossRef](#)]
30. Bayatanova, L.; Rakhadilov, B.; Kurbanbekov, S.; Skakov, D.; Popova, N. Fine structure of low-carbon steel after electrolytic plasma treatment. *Mater. Test.* **2021**, *63*, 842–847. [[CrossRef](#)]
31. Jiang, Y.F.; Bao, Y.F.; Yang, K. Effect of C/N concentration fluctuation on formation of plasma electrolytic carbonitriding coating on Q235. *J. Iron Steel Res. Int.* **2012**, *19*, 39–45. [[CrossRef](#)]
32. Shen, D.J.; Wang, Y.L.; Nash, P.; Xing, G.Z. A novel method of surface modification for steel by plasma electrolysis carbonitriding. *Mater. Sci. Eng. A* **2007**, *458*, 240–243. [[CrossRef](#)]
33. Rastkar, A.R.; Shokri, B. Surface modification and wear test of carbon steel by plasma electrolytic nitrocarburizing. *Surf. Interface Anal.* **2012**, *44*, 342–351. [[CrossRef](#)]
34. Kazerooni, N.A.; Bahrololoom, M.E.; Shariat, M.H.; Mahzoon, F.; Jozaghi, T. Effect of ringer's solution on wear and friction of stainless steel 316L after plasma electrolytic nitrocarburising at low voltages. *J. Mater. Sci. Technol.* **2011**, *27*, 906–912. [[CrossRef](#)]
35. Nie, C.; Zhu, T.; Xie, Y.; Ying, L.; Wang, G. Study on preparation and friction characteristics of steel 1045 modified layer based on plasma electrolytic carbonitriding. *Mater. Today Commun.* **2022**, *33*, 104518. [[CrossRef](#)]
36. Kusmanov, S.A.; Smirnov, A.A.; Silkin, S.A.; Belkin, P.N. Increasing wear and corrosion resistance of low-alloy steel by anode plasma electrolytic nitriding. *Surf. Coat. Technol.* **2016**, *307*, 1350–1356. [[CrossRef](#)]
37. Zarchi, M.K.; Shariat, M.H.; Dehghan, S.A.; Solhjoo, S. Characterization of nitrocarburized surface layer on AISI 1020 steel by electrolytic plasma processing in an urea electrolyte. *J. Mater. Res. Technol.* **2013**, *2*, 213–220. [[CrossRef](#)]
38. Jiang, Y.; Bao, Y.; Wang, M. Kinetic Analysis of Additive on Plasma Electrolytic Boriding. *Coatings* **2017**, *7*, 61. [[CrossRef](#)]
39. Pérez, H.; Vargas, G.; Magdaleno, C.; Silva, R. Oxy-Nitriding AISI 304 Stainless Steel by Plasma Electrolytic Surface Saturation to Increase Wear Resistance. *Metals* **2023**, *13*, 309. [[CrossRef](#)]
40. Kusmanov, S.A.; Kusmanova, Y.V.; Naumov, A.R.; Belkin, P.N. Formation of Diffusion Layers by Anode Plasma Electrolytic Nitrocarburizing of Low-Carbon Steel. *J. Mat. Eng. Perform.* **2015**, *24*, 3187–3193. [[CrossRef](#)]
41. Apelfeld, A.; Borisov, A.; Dyakov, I.; Grigoriev, S.; Krit, B.; Kusmanov, S.; Silkin, S.; Suminov, I.; Tambovskiy, I. Enhancement of Medium-Carbon Steel Corrosion and Wear Resistance by Plasma Electrolytic Nitriding and Polishing. *Metals* **2021**, *11*, 1599. [[CrossRef](#)]
42. Tambovskiy, I.; Mukhacheva, T.; Gorokhov, I.; Suminov, I.; Silkin, S.; Dyakov, I.; Kusmanov, S.; Grigoriev, S. Features of Cathodic Plasma Electrolytic Nitrocarburizing of Low-Carbon Steel in an Aqueous Electrolyte of Ammonium Nitrate and Glycerin. *Metals* **2022**, *12*, 1773. [[CrossRef](#)]
43. Aliofkhazraei, M.; Taheri, P.; Sabour Rouhaghdam, A.; Dehghanian, C. Study of nanocrystalline plasma electrolytic carbonitriding for CP-Ti. *Mater. Sci.* **2007**, *43*, 791–799. [[CrossRef](#)]
44. Qin, Y.; Xiong, D.; Li, J.; Tyagi, R. Corrosion and bio-tribological properties of Ti(CN)_x hard coating on titanium alloy by the pulsed plasma electrolytic carbonitriding process. *Tribol. Int.* **2015**, *82*, 543–550. [[CrossRef](#)]
45. Aliev, M.K.; Sabour, A.; Taheri, P. Corrosion Protection Study of Nanocrystalline Plasma-Electrolytic Carbonitriding Process for CP-Ti. *Prot. Met.* **2008**, *44*, 618–623. [[CrossRef](#)]
46. Aliofkhazraei, M.; Sabour Rouhaghdam, A.; Sabouri, M. Effect of frequency and duty cycle on corrosion behavior of pulsed nanocrystalline plasma electrolytic carbonitrided CP-Ti. *J. Mater. Sci.* **2008**, *43*, 1624–1629. [[CrossRef](#)]
47. Dong, Y.-X.; Chen, Y.-S.; Chen, Q.; Liu, B.; Song, Z.-X. Characterization and blood compatibility of TiC_xN_{1-x} hard coating prepared by plasma electrolytic carbonitriding. *Surf. Coat. Technol.* **2007**, *201*, 8789–8795. [[CrossRef](#)]
48. Shelekhov, E.V.; Sviridova, T.A. Programs for X-ray analysis of polycrystals. *Metal Sci. Heat. Treat.* **2000**, *42*, 309–313. [[CrossRef](#)]
49. Grazulis, S.; Chateigner, D.; Downs, R.T.; Yokochi, A.T.; Le Bail, A. Crystallography open database—An open-access collection of crystal structures. *J. Appl. Crystallogr.* **2009**, *42*, 726–729. [[CrossRef](#)]

Disclaimer/Publisher's Note: The statements, opinions and data contained in all publications are solely those of the individual author(s) and contributor(s) and not of MDPI and/or the editor(s). MDPI and/or the editor(s) disclaim responsibility for any injury to people or property resulting from any ideas, methods, instructions or products referred to in the content.